Retinal Crystals in Type 2 Idiopathic Macular Telangiectasia

Ferenc B. Sallo, MD, PhD,[1,2] Irene Leung, BA,[1] Mina Chung, MD,[3,4] Ute E. K. Wolf-Schnurrbusch, MD,[5] Alfredo Dubra, PhD,[4,6] David R. Williams, PhD,[4] Traci Clemons, PhD,[7] Daniel Pauleikhoff, MD, PhD,[8] Alan C. Bird, MD,[1] Tunde Peto, MD, PhD,[9] on behalf of the MacTel Study Group

Purpose: To characterize the phenotype and investigate the associations of intraretinal crystalline deposits in a large cohort with type 2 idiopathic macular telangiectasia (MacTel).

Design: Case-control study.

Participants: Patients with and without retinal crystals from the Macular Telangiectasia Project, an international multicenter prospective study of type 2 MacTel.

Methods: Grading of stereoscopic 30-degree color fundus (CF), confocal blue light reflectance (CBR), red-free (RF), and infrared (IR) images was performed according to the MacTel Natural History Study protocol and staged using the classification system devised by Gass and Blodi. Spectral domain-optical coherence tomography (SD-OCT) and adaptive optics imaging were used for a finer analysis of the phenotype. Associations between crystals and other characteristics of the disease, as well as potential risk factors, were investigated.

Main Outcome Measures: Presence of crystals, fundus signs of MacTel, clinical characteristics, and presence of potential risk factors of MacTel.

Results: Of 443 probands enrolled in the MacTel study, 203 (46%) had crystalline deposits present; 60% of the cases were bilateral at baseline. Eyes with crystals had a mean letter score of 70.7 (standard deviation [SD] = 15.9), whereas those without crystals had a mean letter score of 66.5 (SD = 15.5, $P < 0.001$). Crystals were present at all stages of the disease and showed high reflectivity within a wide wavelength range. They were located at the anterior surface of the nerve fiber layer, arranged along the nerve fibers, within an annular area centered on the fovea. Significant associations of crystalline deposits were found with a loss of retinal transparency, macular pigment optical density (MPOD) loss, fluorescein leakage, retinal thickness, and a break in the inner segment/outer segment junction line. Associations with environmental risk factors were not found.

Conclusions: Intraretinal crystals are a frequent phenomenon associated with type 2 MacTel. They may appear at all stages and aid in the early diagnosis of the disease. Their morphology further implicates Müller cells in the pathogenesis of the disease. Insight into their physical and chemical properties may provide clues to the metabolic pathways involved in the pathogenesis of the disease.

Financial Disclosure(s): Proprietary or commercial disclosure may be found after the references.
Ophthalmology 2011;118:2461–2467

Idiopathic macular telangiectasia (MacTel) is a vascular anomaly affecting retinal capillaries in the juxtafoveal region.[1] The cause and pathogenesis of the disease are little known.

According to a system originally devised by Gass and Blodi[2] and subsequently simplified by Yannuzzi et al,[3] MacTel is classified into 2 main categories based on biomicroscopic and fluorescein angiographic features. Type 1 (aneurysmal telangiectasia) is a predominantly unilateral disease affecting mostly men, associated clinically with retinal thickening, prominent extensive telangiectasis, lipid exudates, and cystoid changes, mainly in the temporal part of the macula. Type 2 (perifoveal telangiectasia) is a bilateral disease that affects both sexes, starting in the 5th to 7th decades. Early clinical features are more subtle and include a loss of retinal transparency, retinal crystals, intraretinal cystoid spaces at the fovea, and a diffuse leakage in the fluorescein angiogram. The retina is thinner than normal. Subsequent vascular remodeling and fibrosis accompanied by pigment plaques and eventual subretinal neovascularization, scarring, and atrophy limit the prognosis for central vision. The benefit of therapies including anti-vascular endothelial growth factor agents has been explored in several case series, with variable, mostly limited, and transient success. To date, no known therapeutic modality has been proven effective in the long term.[4–8]

The presence of yellow-white refractile crystals in the superficial layers of the parafoveal retina is a characteristic and frequent feature of the disease phenotype.[1,9,10] Their origin, composition, and significance are unknown. Our aim was to characterize the phenotype and associations of these intraretinal crystalline deposits using multiple imaging modalities in a large cohort with type 2 MacTel.

ISSN 0161-6420/11/$–see front matter
doi:10.1016/j.ophtha.2011.05.022

Table 1. Distribution of Probands with Retinal Crystals by Gender and Race

	No Crystals (n=232)		Crystals (n=203)		*P* Value
	n	%	n	%	
Male gender	87	37	83	41	0.47
White race*	193	83	159	78	0.2

*Race was compared with non-Caucasian race given the small numbers in each individual race group. Non-Caucasian races included American Indian, Asian, African American, Native Hawaiian or Pacific Islander, and Australian Aboriginal or Torres Strait Islander. Test: chi-square test.

Materials and Methods

Patients

Patients with a diagnosis of type 2 MacTel with and without retinal crystals from the MacTel project, an international multicenter prospective study of type 2 MacTel, currently involving 28 research centers worldwide, were included in this analysis. The study protocol adhered to the tenets of the Declaration of Helsinki and was approved by the respective institutional review board or local ethics committee at each participating center. Before inclusion, written, informed consent was obtained from each participant after explanation of the nature of the study. Maximum retinal irradiance of lasers used was well below the limits established by the American National Standards Institute (Z136.1; 1993) and other international standards.

Imaging

Standard 30-degree stereo field 2 color fundus (CF) and red-free (RF) images were recorded digitally or digitized at high resolution from color transparencies. Confocal scanning laser ophthalmoscopes (cSLOs) (Heidelberg Retina Angiograph 2 or Spectralis HRA+OCT, Heidelberg Engineering GmbH, Dossenheim, Germany) were used for fundus autofluorescence (FAF), confocal blue light reflectance (CBR), infrared (IR) imaging, and indocyanine green (ICG) angiography. For FAF and CBR imaging, the fundus was illuminated using an excitation light with a wavelength of 488 nm. Fundus autofluorescence was recorded through a filter with a short-wavelength cutoff at 520 nm. To reduce random noise, a master image was produced for each eye in the study by averaging individually recorded images. A standard excitation wavelength of 790 nm was used for ICG angiography, and a diode laser was used to illuminate the fundus at 820 nm for IR imaging. Fluorescein angiography (FA) was performed using a variety of imaging equipment available at respective centers participating in the MacTel study, including cSLOs and fundus cameras. Optical coherence tomography (OCT) of the macula was performed routinely using Stratus OCT-3 (Carl Zeiss Meditec, Inc., Oberkochen, Germany), complemented by high-resolution spectral domain (SD)-OCT imaging where available (Spectralis HRA-OCT, Heidelberg Engineering GmbH). Macular pigment optical density (MPOD) was assessed using a cSLO (Heidelberg Retina Angiograph, Heidelberg Engineering GmbH) through a dual-wavelength (488/514 nm) autofluorescence technique described previously.[11] Additional high-resolution retinal images were obtained with the University of Rochester adaptive optics scanning laser ophthalmoscope (AOSLO).[12,13] Through-focus images of the nerve fiber layer (NFL) and the retinal photoreceptors in the same retinal locations were acquired using near-IR reflectance with <2-μm transverse resolution and 19-Hz video rate. Confocal pinholes of 0.5 to 1.5 Airy disks improved contrast through optical sectioning. The Rochester AOSLO has an 847-nm laser beacon, a Shack–Hartmann wavefront sensor, (The wavefront sensor was a custom Shack-Hartmann sensor with a Rolera-XR camera from Qimaging [Surrey, British Columbia, Canada], a 200 micron pitch, 7.0 mm focal length lenslet array from Adaptive Optics Associates [Northrop Grumman Corporation, Cambridge, MA], and an 847 nm fiber-coupled laser diode from Qphotonics [Ann Arbor, MI] as beacon) and an Alpao hi-speed 97 actuator deformable mirror (Alpao S.A.S. [Biviers, Grenoble, France]). The scanning system has an adjustable 0.75- to 2.5-degree field of view. Infrared reflectance imaging of the retina was achieved with a 680-nm superluminescent diode source and a photomultiplier tube for light detection. The raw data were registered and frame averaged using custom Matlab software (MathWorks, Inc., Natick, MA), and individual frames were montaged using Adobe Photoshop (Adobe Systems Inc., San Jose, CA).

Phenotyping

Detailed phenotyping based on the Gass and Blodi[2] classification was performed by grading of field 2 CF, RF, and FA images, according to the system defined in the MacTel Study protocol.[14] Briefly, a grid (adapted from the standard grid for age-related maculopathy classification[15,16] consisting of 3 concentric circles with 1000-, 3000-, and 6000-μm diameters and 4 radial quadrant spokes dividing the central macula into 9 subfields) was superimposed over the CF image, centered on the fovea, in Adobe Photoshop CS4 (Adobe Systems Inc.). Images were graded for image quality and fundus features of type 2 MacTel listed in Table 1, and for OCT and FAF characteristics as described previously.[14] Grading was performed independently by 3 certified graders masked to the identity and clinical data of the patients. Gradings were compared for inter- and intraobserver reliability, and final copy was created by adjudication. Staging of disease severity was based on the criteria devised by Gass and Blodi[2] using the categories shown in Table 2.

Registration of Retinal Crystals

In cases where grading detected the presence of crystals, composite images containing overlays of aligned CF, CBR, RF, and IR

Table 2. Associations with Fundus Autofluorescence and Optical Coherence Tomography Characteristics

	No Crystals %	Crystals %	*P* value
Abnormal foveal avascular zone	89	85	0.4
Inner empty spaces	46	50	0.29
Outer empty spaces	18	24	0.09
Inner empty spaces			0.45
Center not involved	25	25	
Center involved	20	24	
Outer empty spaces			0.13
Center not involved	10	17	
Center involved	7	7	
Inner segment/outer segment junction line break	50	68	<0.001
Increased autofluorescence within 1 DD of the fovea	80	83	0.47
Fovea abnormal	85	83	0.72
Large area of decreased autofluorescence	7	8	0.65

DD = disc diameter.
Test: chi-square test.

images were created (in Adobe Photoshop CS4) and analyzed for the presence and location of crystals in images of respective modality. The number of crystals present per subfield within the grading grid was assessed in each imaging modality and graded using the categories 0, 1–5, 6–10, and >10.

Clinical Data Collection

Clinical information, including age, gender, self-reported race/ethnicity, and medical and ocular history, was collected through standardized questionnaires.[14] Monocular best-corrected visual acuities were determined according to a standardized protocol using the Early Treatment Diabetic Retinopathy Study logarithm of the minimum angle of resolution visual acuity charts at a distance of 4 m. Scoring of the test was based on the number of letters read correctly. Possible scores ranged from 0 (Snellen equivalent <20/800) to 100 (Snellen equivalent 20/12).[17,18] Participants also underwent an annual comprehensive ophthalmologic examination.[14] Evaluation of vision-targeted health-related quality of life was measured using the National Eye Institute Visual Functioning Questionnaire-25.[19]

Statistical Methods

Comparisons of various characteristics of interest between participants/eyes with and without crystalline deposits were performed using a chi-square test. Generalized linear models were used to compare continuous image grading characteristics across the crystalline deposit groups. Kappa statistics were used to assess the agreement of the crystalline deposit grading across the various image modalities. A P value of <0.05 was accepted as statistically significant. All analyses were conducted using commercially available statistical software (SAS version 9.1; SAS Inc., Cary, NC).

Results

Demographics

Of 443 patients enrolled in the MacTel study, 203 (46%) showed crystalline deposits. At enrollment, the mean age of patients with crystals was 60.0 years (standard deviation [SD] = 8.8), and the mean age of patients without crystals was 60.4 years (SD = 9.8).

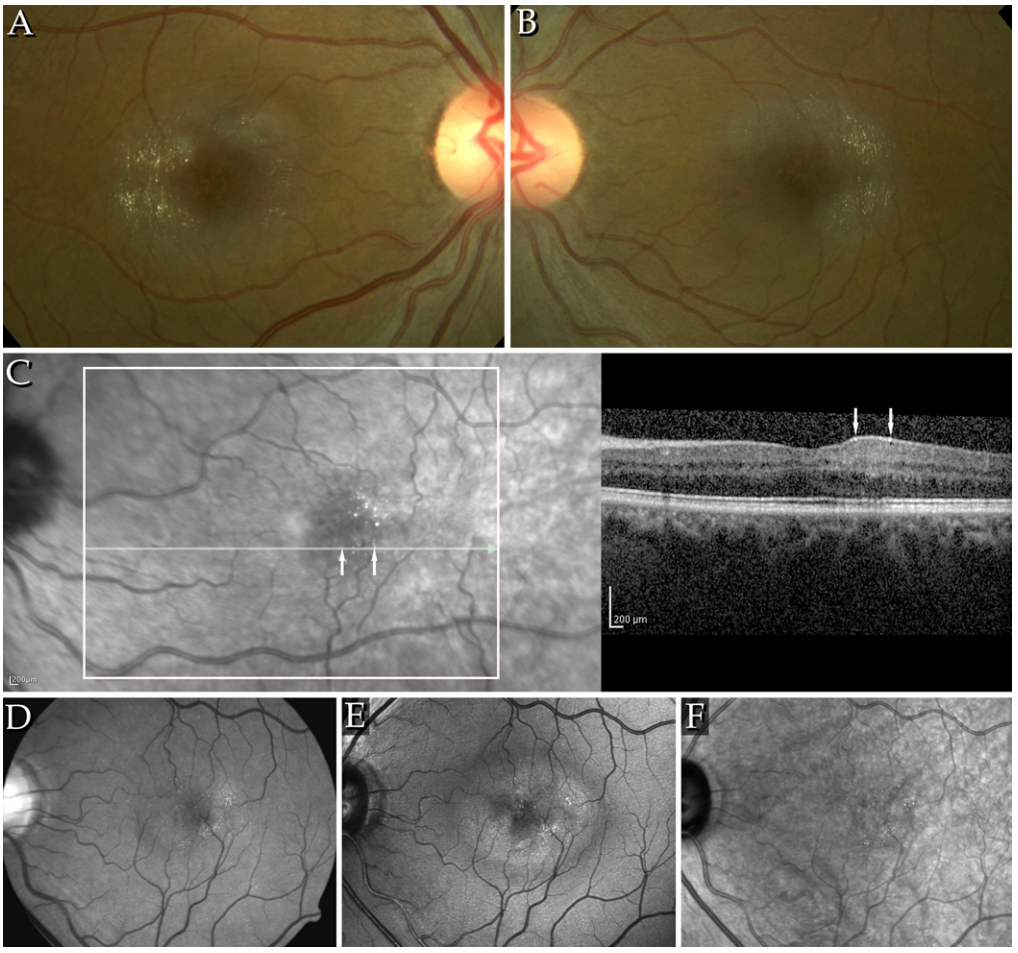

Figure 1. A, B, The CF images of the right and left eyes of a patient with signs of stage 3 MacTel, including retinal crystals. The crystals are arranged in a pattern along the fibers of the NFL, within a round area with an approximate diameter of up to 4000 μm, centered on the fovea. Typically, few crystals are seen at and immediately around the fovea. The area temporal of the fovea, corresponding to the raphe, usually contains less crystals. **C,** An IR+OCT image combination from the Heidelberg Spectralis (Heidelberg Engineering GmbH, Dossenheim, Germany). Arrows indicate identical retinal crystals in the IR image and B-scan. The crystals appear to be located in the NFL. **D–F,** Detectability of crystals in different imaging modalities: **D,** An RF image taken with a fundus camera. **E, F,** Confocal blue light reflectance and IR images (Heidelberg Spectralis HRA+OCT). Best detectability of crystals is provided by the CBR images. Crystals were located within the area of increased reflectivity in CBR.

Figure 2. The AOSLO images of the left eye of a 60-year-old patient with MacTel, visual acuity 20/25. **A,** Montage of AOSLO images on standard 30-degree fundus photograph. **B,** Distribution of crystals appears to be parallel to the ganglion cell axon bundles within the NFL. **C,** Individual crystals appear with high contrast in the same focal plane as the NFL. **D,** The cone mosaic at the same retinal location appears regular with no evidence of crystals at this focal plane. Scale bars = 50 μm.

Follow-up periods ranged from 0 to 4 years with a mean of 1.6 years (median = 2, SD = 1.2 years). The distributions by gender and race are shown in Table 1.

Phenotype

At baseline, of 203 participants showing retinal crystals, 121 (59.6%) were bilateral and 81 (39.9%) were unilateral. Retinal crystals were located within a band approximately 4000 μm in diameter centered on the fovea, with a sparing of approximately 700 μm around the center of the fovea. In 34 cases (16.8%), a pattern in the alignment of the crystals corresponding to that of the NFL was clearly distinguishable in fundus images (Figs 1A, B and 2B, C). In 78% of cases with an NFL pattern, a gap in the pattern temporal of the fovea corresponding to the raphe was apparent (Fig 1A, B). High-resolution imaging using AOSLO confirmed this pattern and the presence of the crystals within the same optical section as the nerve fiber bundles (Fig 2). Individual crystals were least 5 μm or larger. Crystals appeared to be angular with sharply demarcated edges and were distributed in a distinct to subconfluent pattern. On the basis of the analysis of stereoscopic fundus images, retinal crystals appeared to be located at the inner surface of the retina. This observation was confirmed by SD-OCT imaging; crystals appeared within the NFL (Fig 1C).

In CF images the crystals appeared highly reflective, white, or golden yellow. Crystals were also detectable in RF, CBR, and IR images. Agreement of crystal counts grading based on CF images (in the temporal zone 2 subfield) was substantial with RF κ=0.80 (0.77–0.83) and CBR κ=0.69 (0.63–0.75) images, and moderate with IR images κ=0.47 (0.41–0.54). Values shown are weighted kappa values and 95% confidence intervals in parentheses. Red-free and CBR imaging provided the highest detection rates, whereas only a subset of crystals was typically seen in IR images. Crystals were not detectable in FA, FAF, or ICG images.

Crystals were seen at all stages of the disease, most frequently in stages 3 and 4. The association of the amount of crystals with Gass and Blodi[2] stage reached significance in zone 1 (P=0.003) and the temporal subfield of zone 2 (P=0.035, Fisher exact test).

Associations with Features of the Phenotype

The presence of crystals showed a strong association with the presence of a break in the inner segment/outer segment junction line but not with other FAF/OCT characteristics of the disease (Table 2).

The amount of crystals showed a statistically significant association with loss of retinal transparency and fluorescein leakage in all subfields and with retinal thickness except in zone 1 and temporal zone 2 (Tables 3 and 4, available at http://aaojournal.org). The association with visible telangiectatic vessels, dilated retinal vessels, and right-angled veins only reached significance in the nasal subfield of zone 2 (P=0.002, P=0.04, and P=0.03, respectively). No association was found with blunted veins. Associations with MPOD loss were significant in all subfields except the inferior subfield of zone 2 (zone 1 P=0.04, zone 2: superior P=0.009, nasal P=0.02, inferior P=0.08, and temporal P=0.001, n=52 eyes).

Associations with Clinical Features

Eyes with crystals (n=520) had a mean letter score of 70.7 (SD = 15.9), and eyes without crystals (n=343) had a mean letter score of 66.5 (SD = 15.5). The differences were significant ($P < 0.001$). Associations with diet or other clinical characteristics were not detectable (Table 5).

Table 5. Associations with Clinical Characteristics

	No Crystals N=232	Crystals N=200	*P* Value
Diabetes	68 (29)	74 (37)	0.09
Cerebral vascular incident	6 (3)	3 (2)	0.43
Coronary artery disease	23 (10)	29 (14)	0.14
Hypertension	127 (55)	103 (51)	0.5
Smoking*			
Never	110 (48)	102 (51)	0.39
Former	94 (41)	71 (36)	
Current	23 (10)	26 (13)	
Medication exposure†			
Cholesterol-lowering agents	88 (39)	80 (40)	0.73
Tamoxifen	6 (3)	6 (3)	0.81
Vitamins	89 (39)	82 (41)	0.64
Dietary supplements	65 (29)	59 (30)	0.79
Multivitamin	56 (25)	40 (20)	0.27
Preservision	13 (6)	19 (10)	0.13
Vitamin A	3 (1)	6 (3)	0.22
Beta-carotene	3 (1)	3 (2)	0.87
Zinc	4 (2)	7 (4)	0.25
Lutein/zeaxanthin	13 (6)	13 (7)	0.72
NEI-VFQ			
Overall NEI-VFQ score	77.9 (13.7)	78.1 (13.6)	0.17
General vision	65.6 (15.7)	64.6 (62.4)	0.52
Color vision	96.7 (10.8)	96.8 (11.0)	0.9
Near activities	70.9 (20.2)	67.4 (20.6)	0.08
Distance activities	76.9 (19.2)	75.3 (21.3)	0.41

NEI-VFQ = National Eye Institute Visual Function Questionnaire.
Values are n (probands) with % shown in parentheses, or mean ± SD for the NEI-VFQ data. Note 3 participants did not have these data available. Chi-square test was used for comparing percentages; *t* test was used for comparing means.
*Smoking data not available for 9 participants (4 with and 5 without crystals).
†Data not available for 10 participants (5 with and 5 without crystals).

Discussion

Retinal crystals may be present in a wide range of disorders from hereditary to drug-induced and from systemic to local retinal.[20,21] In type 2 MacTel, retinal crystals have some distinguishing characteristics.[1,2,9,10]

In our study, retinal crystals were present in 46% of 443 patients with MacTel at baseline, and approximately two thirds of these cases were bilateral. Crystals appeared highly reflective at wavelengths ranging from 488 nm (blue) to 820 nm (IR). In IR images, typically only a subset of crystals seen in CBR or RF images were detectable. In view of the confocal characteristics of the SLO, this may simply be due to a tilt of the retina relative to the focal plane. The crystals also exhibited specular reflection such that multiple frames of the same retinal area taken at slightly different angles showed a variation in the number and location of the crystals. As a rule, more crystals are likely to be present in the retina than those detectable in any single fundus image.

Retinal crystals in MacTel are typically distributed in an annular pattern within an ~4000-μm diameter circular area centered on the fovea, with a sparing of the central area of ~700 μm. A gap in this annular pattern was seen temporal of the fovea, corresponding to the horizontal raphe. This is remarkable because many other signs of the disease appear first or occur predominantly in this region.

Within this annular area, the crystals were arranged along the ganglion cell axons in the NFL. To our knowledge, this pattern of crystals is only seen in MacTel and Sjögren–Larsson Syndrome (SLS).[22,23] At late stages of MacTel, the distortion of the retina due to vascular remodeling, fibrosis, and pigment plaques may break up this pattern. In some late-stage eyes, only a few crystals were apparent surrounding the pigment plaques or fibrotic postneovascular scars. This pattern has been reported in other neovascular conditions and is thus probably not specific for MacTel.[24]

The retinal area affected by crystals coincides closely with that affected by other features of the disease. A circumfoveal band of increased reflectivity seen in CBR images, the loss of retinal transparency in CF and RF images, the loss of macular pigment, and fluorescein leakage all seem to affect this region. In our study, the amount of crystals showed statistically significant associations with the loss of retinal transparency, loss of MPOD, and fluorescein leakage.

The implications of these observations are not known, but they suggest further Müller cell involvement in the pathogenesis of type 2 MacTel. Müller cells are radially oriented support cells traversing the retina from the inner vitreal border to the distal end of the outer nuclear layer. They have an extended funnel shape and a higher refractive index than their surrounding tissue and are oriented along the direction of light propagation. Müller cells have been shown to act as optical fibers within the retina.[25] A disruption of their structure may explain a loss of retinal transparency even without significant edema. In our study, retinal crystals did however also show a statistically significant association with a minimal level of retinal thickening in all subfields.

The cell processes of Müller cells enclose regions of the perikarya and fascicles of axons of the ganglion cells within the NFL; processes from their footplates surround the nerve fiber bundles.[26] In our study, high-resolution retinal images obtained using adaptive optics confirmed our findings. On stereoscopic fundus images and SD-OCT imaging, crystals seem to be located superficially within the NFL, in close proximity of the nerve fibers. Individual ganglion cell axon diameters vary from 0.6 to 2.0 μm depending on the type of ganglion cell of their origin. Midget ganglion cells with thinner axons are found more frequently within the macular area.[27] We estimate that individual crystals are ~5 μm or larger. This, together with their often confluent distribution, suggests that crystals are more likely to be located around the nerve fiber bundles, possibly within Müller cell footplates, rather than within individual axons. A similar conclusion was drawn in the case of tamoxifen crystals, and other crystals, such as canthaxanthin and beta-carotene, also form in the innermost retina.

Müller cells play a role in retinoid metabolism, including cone pigment regeneration, and show avid phagocytic activity.[28] Although the origin and chemical composition of the crystals are not known, according to their distribution and reflective properties, we hypothesize that they may be composed of retinoids originating in the visual cycle and may be

located within the Müller cell footplates and processes surrounding the nerve fibers. We also found a significant association between the amount of crystals and the presence of a break in the inner segment/outer segment junction line, which may further support this hypothesis; however, significant associations with increased retinoid intake via the diet or supplementation were not demonstrated in our study.

We found an association between the amount of crystals and the fluorescein leakage. Macular pigment loss was also associated with the amount of retinal crystals in our study. Müller cells extend branches that interdigitate with retinal neurons and glial cells, and their processes ensheathe the retinal capillaries and may contribute to the blood–retina barrier.[26] The role of Müller cells in the metabolism of macular pigment is not clear; however, in a histologic study of a MacTel eye, Powner et al[29] found a depletion of Müller cells and vascular abnormalities within an area of the same extent as the loss of macular pigment. The distribution and associations of retinal crystals found in our study thus further implicate Müller cells in the pathogenesis of MacTel.

The reflective properties of the crystals are compatible with those of retinoids but also with those of lipids. Retinal crystals arranged along the nerve fibers, central cystoid spaces, and a loss of luteal pigment seen in MacTel are also the ocular manifestations of SLS, which raises the possibility of similarities in the metabolic pathways responsible for the pathogenesis of the 2 diseases. Sjögren–Larsson Syndrome is an autosomal dominant hereditary systemic metabolic disorder characterized by deficient microsomal fatty aldehyde dehydrogenase activity, resulting in an accumulation of fatty aldehydes and alcohols in body tissues; however, SLS is also associated with severe extraocular manifestations, including cognitive deficiencies, spastic diplegia, and congenital ichtyosis.[22,23]

In conclusion, further insight into the physical and chemical properties of retinal crystals in MacTel may provide clues to the metabolic pathways involved in the pathogenesis of the disease.

Acknowledgments. The authors thank Drs. Marcus Fruttiger and Austin Roorda for valuable discussions concerning the microanatomic and optical aspects of the crystals, respectively.

References

1. Gass JD, Oyakawa RT. Idiopathic juxtafoveolar retinal telangiectasis. Arch Ophthalmol 1982;100:769–80.
2. Gass JD, Blodi BA. Idiopathic juxtafoveolar retinal telangiectasis. Update of classification and follow-up study. Ophthalmology 1993;100:1536–46.
3. Yannuzzi LA, Bardal AM, Freund KB, et al. Idiopathic macular telangiectasia. Arch Ophthalmol 2006;124:450–60.
4. Gamulescu MA, Walter A, Sachs H, Helbig H. Bevacizumab in the treatment of idiopathic macular telangiectasia. Graefes Arch Clin Exp Ophthalmol 2008;246:1189–93.
5. Kovach JL, Rosenfeld PJ. Bevacizumab (Avastin) therapy for idiopathic macular telangiectasia type II. Retina 2009; 29:27–32.
6. Matsumoto Y, Yuzawa M. Intravitreal bevacizumab therapy for idiopathic macular telangiectasia. Jpn J Ophthalmol 2010; 54:320–4.
7. Charbel Issa P, Finger RP, Holz FG, Scholl HP. Eighteen-month follow-up of intravitreal bevacizumab in type 2 idiopathic macular telangiectasia. Br J Ophthalmol 2008;92: 941–5.
8. Charbel Issa P, Finger RP, Kruse K, et al. Monthly ranibizumab for nonproliferative macular telangiectasia type 2: a 12-month prospective study. Am J Ophthalmol 2011;151: 876–86.
9. Moisseiev J, Lewis H, Bartov E, et al. Superficial retinal refractile deposits in juxtafoveal telangiectasis. Am J Ophthalmol 1990;109:604–5.
10. Abujamra S, Bonanomi MT, Cresta FB, et al. Idiopathic juxtafoveolar retinal telangiectasis: clinical pattern in 19 cases. Ophthalmologica 2000;214:406–11.
11. Helb HM, Charbel Issa P, van der Veen RL, et al. Abnormal macular pigment distribution in type 2 idiopathic macular telangiectasia. Retina 2008;28:808–16.
12. Gomez-Vieyra A, Dubra A, Malacara-Hernandez D, Williams DR. First-order design of off-axis reflective ophthalmic adaptive optics systems using afocal telescopes. Opt Express 2009;17:18906–19. Available at: http://www.opticsinfobase.org/abstract.cfm?URI=oe-17-21-18906. Accessed May 3, 2011.
13. Scoles D, Gray DC, Hunter JJ, et al. In-vivo imaging of retinal nerve fiber layer vasculature: imaging histology comparison. BMC Ophthalmol 2009;9:9. Available at: http://www.biomedcentral.com/1471-2415/9/9. Accessed May 3, 2011.
14. Clemons TE, Gillies MC, Chew EY, et al. Baseline characteristics of participants in the natural history study of macular telangiectasia (MacTel) MacTel Project Report No. 2. Ophthalmic Epidemiol 2010;17:66–73.
15. Bird AC, Bressler NM, Bressler SB, et al. An international classification and grading system for age-related maculopathy and age-related macular degeneration. The International ARM Epidemiological Study Group. Surv Ophthalmol 1995;39: 367–74.
16. Klein R, Davis MD, Magli YL, et al. The Wisconsin age-related maculopathy grading system. Ophthalmology 1991;98: 1128–34.
17. Ferris FL 3rd, Kassoff A, Bresnick GH, Bailey I. New visual acuity charts for clinical research. Am J Ophthalmol 1982;94: 91–6.
18. Early Treatment Diabetic Retinopathy Study design and baseline patient characteristics. ETDRS report number 7. Ophthalmology 1991;98:741–56.
19. Clemons TE, Gillies MC, Chew EY, et al. The National Eye Institute Visual Function Questionnaire in the Macular Telangiectasia (MacTel) Project. Invest Ophthalmol Vis Sci 2008; 49:4340–6.
20. Drenser K, Sarraf D, Jain A, Small KW. Crystalline retinopathies. Surv Ophthalmol 2006;51:535–49.
21. Nadim F, Walid H, Adib J. The differential diagnosis of crystals in the retina. Int Ophthalmol 2001;24:113–21.
22. van der Veen RL, Fuijkschot J, Willemsen MA, et al. Patients with Sjogren-Larsson syndrome lack macular pigment. Ophthalmology 2010;117:966–71.
23. Fuijkschot J, Cruysberg JR, Willemsen MA, et al. Subclinical changes in the juvenile crystalline macular dystrophy in Sjogren-Larsson syndrome detected by optical coherence tomography. Ophthalmology 2008;115:870–5.
24. Lima LH, Freund KB, Klancnik JM Jr, Spaide RF. Intraretinal crystalline deposits in neovascular age-related macular degeneration. Retina 2010;30:542–7.
25. Franze K, Grosche J, Skatchkov SN, et al. Muller cells are living optical fibers in the vertebrate retina. Proc Natl Acad Sci U S A 2007;104:8287–92.

26. Sarthy V, Ripps H. Structural organization of retinal glia. In: Blakemore C, ed. The Retinal Müller Cell: Structure and Function. New York: Kluwer Academic/Plenum Publishers; 2001:5–27.
27. Hogan MJ, Alvarado JA, Weddell JE. Retina. In: Hewes J, ed. Histology of the Human Eye: An Atlas and Textbook. Philadelphia, PA: Saunders; 1971:393–519.
28. Sarthy V, Ripps H. Metabolic interactions with neurons. In: Blakemore C, ed. The Retinal Müller Cell: Structure and Function. New York: Kluwer Academic/Plenum Publishers; 2001:95–100.
29. Powner MB, Gillies MC, Tretiach M, et al. Perifoveal muller cell depletion in a case of macular telangiectasia type 2. Ophthalmology 2010;117:2407–16.

Footnotes and Financial Disclosures

Originally received: March 9, 2011.
Final revision: May 12, 2011.
Accepted: May 16, 2011.
Available online: August 12, 2011. Manuscript no. 2011-403.

[1] Moorfields Eye Hospital, NHS Foundation Trust, London, United Kingdom.

[2] UCL Institute of Ophthalmology, London, United Kingdom.

[3] Flaum Eye Institute, University of Rochester, Rochester, New York.

[4] Center for Visual Science, University of Rochester, Rochester, New York.

[5] Universtätsklinik für Augenheilkunde, University of Bern, Switzerland.

[6] The Institute of Optics, University of Rochester, New York, New York.

[7] The EMMES Corporation, Rockville, Maryland.

[8] St. Franziskus Hospital, Münster, Germany.

[9] NIHR Biomedical Research Centre for Ophthalmology at Moorfields Eye Hospital, NHS Foundation Trust and UCL Institute of Ophthalmology, London, United Kingdom.

Financial Disclosure(s):
The author(s) have made the following disclosure(s): FBS, IL, MC, UEKW-S, TC, and AD: none. DRW received lecturer fees from GlaxoSmithKline and Alcon; The University of Rochester holds unlicensed patents. DP has acted as a consultant/advisor to Novartis, Bayer, and Allergan. ACB and TP: none.

Funding: The Lowy Medical Foundation and the National Institute for Health Research provided support for this study.

This article contains online-only material: Tables 3 and 4.

Correspondence:
Ferenc B. Sallo, MD, PhD, The Reading Centre, Department of Research and Development, Moorfields Eye Hospital NHS Foundation Trust, 162 City Road, London, EC1V 2PD, UK. E-mail: Ferenc.Sallo@moorfields.nhs.uk.